AIAA JOURNAL
Vol. 30, No. 12, December 1992

Quasiconical Flowfield Structure of the Three-Dimensional Single Fin Interaction

Doyle D. Knight* and Dias Badekas†
Rutgers University, New Brunswick, New Jersey 08903
C. C. Horstman‡
NASA Ames Research Center, Moffett Field, California 94035
and
Gary S. Settles§
Pennsylvania State University, University Park, Pennsylvania 16802

A series of conical and three-dimensional computations have been performed for the swept oblique shock wave/turbulent boundary-layer interaction generated by a 20-deg sharp fin at Mach 4 and Reynolds number $Re_{\delta\infty} = 2.18 \times 10^5$ based on the incoming boundary-layer thickness δ_∞. The Reynolds-averaged compressible Navier-Stokes equations are employed with turbulence incorporated using the Baldwin-Lomax and Jones-Launder models. The computed results are basically similar for both turbulence models and display general agreement with experimental data for surface pressure and surface flow direction, although underestimating the size of the primary vortex. The computed three-dimensional flowfield displays quasiconical behavior of the surface pressure, surface flow direction, and flowfield contours of static pressure, density, and Mach number over the extent of the computational domain except for an inception region near the fin leading edge. The streamlines of the computed three-dimensional flowfield are qualitatively conical; however, the computed attachment streamline does not exhibit conical behavior within the computational domain. The surface skin friction is not conical. Most of the features of the quasiconical flowfield model of Settles et al. are observed in the computations, including the λ shock, slip line, primary vortex, expansion region, and high-speed jet impingement. Certain features of the flowfield model are not observed in the computations, namely, a "normal" shock near the attachment line, transonic shocklets in the expansion region, and secondary separation. The absence of these features in the computation is believed to be indirectly attributable to limitations in the turbulence models.

Introduction

An important problem in modern high-speed fluid mechanics is the interaction of shock waves with turbulent boundary layers. Commonly observed in a wide range of applications in aerodynamics and propulsion, shock wave/turbulent boundary-layer interactions have a significant effect on peak heating loads, aerodynamic performance, and propulsion efficiency. A series of recent reviews by Settles and Dolling[1,2] and Zheltovodov et al.[3-5] provide a general background and describe areas of current research interest.

Many aspects of the basic fluid physics of three-dimensional shock wave/turbulent boundary-layer interaction have been elucidated by theoretical (analytical and computational) and experimental examination of the phenomenon in simplified geometries representative of subsections of realistic engineering configurations. An example is the three-dimensional single sharp fin (Fig. 1) that is the subject of the present paper. This configuration represents a geometrical simplification of a fin-fuselage juncture.

Recent experimental studies of the three-dimensional single fin have been performed by Kim and Settles,[6] Kim et al.,[7] Kubota and Stollery,[8] Law,[9] McClure and Dolling,[10] Oskam et al.,[11,12] Shapey and Bogdonoff,[13] and Zheltovodov et al.[3] Computational studies have been performed by Horstman and Hung,[14] Knight,[15-18] Knight et al.,[19] and Gaitonde and Knight.[20,21] The theoretical models are the three-dimensional Reynolds-averaged compressible Navier-Stokes equations with turbulence incorporated through an algebraic or two-equation eddy viscosity model (e.g., Baldwin-Lomax,[22] Cebeci-Smith,[23] and Jones-Launder[24]). For p_2/p_1 less than approximately four, the theoretical models have demonstrated good agreement with experimental data (e.g., surface pressure, surface flow visualization, and boundary-layer profiles of pitot pressure and yaw angle). In particular, Knight et al.[19] observed close agreement between theory and experiment for the single fin at Mach 3 and $\alpha = 20$ deg, corresponding to $p_2/p_1 = 3.8$, based on an extensive comparison of boundary-layer and surface profiles.

The first objective of this paper is the assessment of the accuracy of the Baldwin-Lomax and Jones-Launder models for a stronger interaction, namely, the three-dimensional single fin at Mach 3.96 and $\alpha = 20$ deg, corresponding to

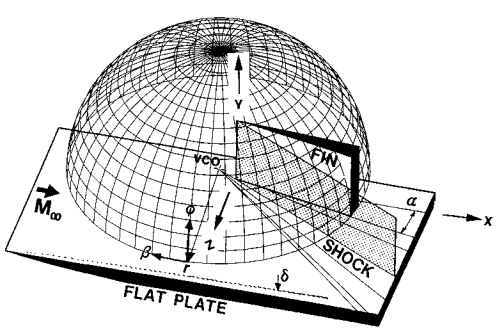

Fig. 1 Three-dimensional sharp fin.

Received Oct. 7, 1991; revision received April 3, 1992; accepted for publication April 3, 1992.

*Professor of Aerospace and Mechanical Engineering, Department of Mechanical and Aerospace Engineering. Associate Fellow AIAA.
†Graduate Research Assistant, Department of Mechanical and Aerospace Engineering.
‡Senior Scientist, Experimental Fluid Dynamics. Associate Fellow AIAA.
§Professor of Mechanical Engineering, Department of Mechanical Engineering, and Director, Gas Dynamics Laboratory. Associate Fellow AIAA.

$p_2/p_1 = 5.15$. The computed flowfields are compared with the experimental data of Kim et al.,[7] including surface pressure and surface flow direction, and the experimental data of Hsu and Settles[25,26] for flowfield density.

The second objective is the examination of the extent of conical symmetry in the computed flowfield at Mach 3.96 and $\alpha = 20$ deg. Many experiments[1-4] have observed conical symmetry of the surface pressure and surface flow patterns outside of an initial inception zone around the fin leading edge. By reducing the dimensionality of the flowfield from three to two, conical symmetry provides a powerful framework for understanding the flowfield. It is therefore important to quantify the nature and extent of conical behavior of the computed flowfields.

The third objective is the examination of the flowfield structure. Following the early work of Stanbrook,[27] Lowrie,[28] and McCabe,[29] Token[30] postulated a large vortex structure on the flat plate. Later, Kubota and Stollery[8] noted an additional (counter-rotating) vortex in the corner. Zheltovodov[31] proposed a qualitative model incorporating a λ shock and vortex. Knight et al.[19] confirmed the existence of the dominant vortex (for interactions exhibiting flow separation) and described the topology of the separation and attachment surfaces that distinguished the fluid entrained into the vortex from the remainder of the flowfield. Knight et al.[32] further demonstrated that the dominant vortex was the principal feature of the swept compression corner (for interactions exhibiting flow separation) and provided further information about the extent of entrainment into the vortex.[33] Recently, Settles and Dolling,[2] Lu and Settles,[34] and Alvi and Settles[35,36] developed a detailed quasiconical flowfield model. The third objective of this paper is to compare the conical computations with that flowfield model.

Theoretical Models

The theoretical models are the full three-dimensional compressible Reynolds-averaged Navier-Stokes equations[37] (RANS) in strong conservation form[38] with turbulence incorporated through the turbulent eddy viscosity models of Baldwin and Lomax, and Jones and Launder. Additionally, computations have been performed using the Baldwin-Lomax model in a conical version of the RANS that was obtained from the three-dimensional RANS under the assumption of conical flow, i.e., the velocity, pressure, and temperature are independent of a spherical radial distance R measured with respect to a virtual conical origin (VCO) that is typically close to the leading edge of the fin (Fig. 1). The Baldwin-Lomax model was implemented as originally proposed[22] with the following modifications: 1) the length scale ℓ was specified by the Buleev formula[15,39] $\ell = 2\,y\tilde{z}/[y + \tilde{z} + (y^2 + \tilde{z}^2)^{1/2}]$ downstream of the fin leading edge where $\tilde{z} = z \cos\alpha$, 2) the eddy viscosity was implemented by dividing the y-z plane into two regions[15,39] adjacent to the flat plate and fin, 3) the wake formulation for the outer eddy viscosity was not employed, and 4) the location of the maximum in the outer function for the outer eddy viscosity (in the region adjacent to the flat plate) was restricted to $y \le \kappa\delta_\infty$, where κ increased from 1 to 2 from the upstream to the downstream boundaries, to avoid selection of spurious peaks outside the boundary layer. The Jones-Launder model was implemented as originally proposed[24] except that the constants $C_{\epsilon 1}$ and $C_{\epsilon 2}$ were modified to 1.44 and 1.92, respectively. The Jones-Launder model was integrated to the wall using the original low Reynolds number model.[24] The molecular dynamic viscosity was specified by Sutherland's law.[40] The molecular and turbulent Prandtl numbers were 0.73 and 0.9, respectively.

Numerical Algorithms

Two different numerical algorithms were employed. The computations of the three-dimensional conical RANS equations using the Baldwin-Lomax turbulence model employed a vectorized hybrid explicit-implicit[15] algorithm incorporating the explicit method of MacCormack[41] and the implicit box scheme of Keller.[42] The computations of the three-dimensional RANS equations using the Jones-Launder model employed the hybrid explicit-implicit algorithm of MacCormack.[43] These algorithms have been extensively employed for the computation of two-dimensional and three-dimensional flows with strong viscous-inviscid interaction and flow separation. The governing equations are integrated in time from an assumed initial condition until a steady-state solution is achieved. The initial condition is the upstream boundary-layer profile that is propagated to all interior locations. Steady state is assumed to be reached when the average relative change in the flow variables (e.g., density, velocity, and total energy) is less than 0.1% over one characteristic time t_c, where $t_c = L/V_\infty$ is the relevant flow development time for the computation. For the three-dimensional calculations, L is the streamwise length of the computational domain and V_∞ is the freestream velocity. For the conical calculations, L is the largest dimension of the computational domain, and V_∞ is the freestream speed of sound.

Details of Computations

Six computations[44,45] have been performed for the single fin at Mach 3.96 and $\alpha = 20$ deg corresponding to the experiments of Kim et al.[7] The Reynolds number $Re_{\delta\infty}$ is 2.18×10^5 ($\delta_\infty = 0.3$ cm), and the wall temperature T_w is nearly adiabatic ($T_w = 1.05\ T_{\text{adiabatic}}$). The computations are summarized in Table 1.

The grids for the three-dimensional computations (cases 1 and 2), described in Table 2, provide an accurate resolution of the flowfield based on previous three-dimensional calculations.[15-17,19] The boundary layers on the flat plate and fin were accurately resolved with the exception of the fin boundary layer for case 2. (Since the boundary layer on the fin surface is quite small, compared with the boundary layer on the flat plate, the insufficient resolution of the fin boundary layer in case 2 does not affect the comparison with experimental data on the flat plate.) The viscous sublayers were accurately resolved with $\Delta y^+ \le 1.4$ and $\Delta z^+ \le 2.2$ for case 1 and

Table 1 Summary of computations

Case no.	Type	Turbulence model	N_1[a]	N_2[b]	N_3[c]	Total points	t_{total}/t_c[d]	Computer	CPU hr
1	Three dimensional	B-L[e]	64	48	72	218,880	5	CYBER 205	5.3
2	Three dimensional	J-L[e]	64	40	64	163,840	4	Cray X-MP	32.0
3	Conical	B-L	n/a	48	60	2,856	41	Cray Y-MP	0.4
4	Conical	B-L	n/a	50	60	2,976	41	Cray Y-MP	0.4
5	Conical	B-L	n/a	83	105	8,691	46	Cray Y-MP	1.2
6	Conical	B-L	n/a	140	208	29,096	45	Cray Y-MP	2.8

[a] N_1—number of planes in x direction for three dimensions, not applicable (n/a) for conical calculations.
[b] N_2—number of planes in y direction for three dimensions or number of points in ϕ direction for conical.
[c] N_3—number of planes in z direction for three dimensions or number of points in β direction for conical.
[d] t_{total}—total physical time of integration; t_c—approximate characteristic time scale of development of flow to steady state (see text). The total number of points for all cases (except no. 2) differs from the product $N_1N_2N_3$ because of the use of a separate refined grid in the immediate vicinity of the corner formed by the fin and flat plate.
[e] B-L—Baldwin-Lomax; J-L—Jones-Launder.

Table 2 Details of the three-dimensional computations

Case no.	Turbulence model	$\Delta x/\delta_\infty$,[a]	$\Delta y/\delta_\infty$,[a] min ($\times 10^3$)	$\Delta y/\delta_\infty$,[a] max	$\Delta z/\delta_\infty$,[a] min ($\times 10^3$)	$\Delta z/\delta_\infty$,[a] max	Δy^+,[b] mean	Δy^+,[b] max	Δz^+,[b] mean	Δz^+,[b] max
1	B-L	0.67	0.40	0.55	0.67	1.09	0.49	1.40	1.70	2.20
2	J-L	0.67	0.25	0.50	57.0	0.50	0.40	0.80	40.0	63.0

[a]Δx, Δy, Δz—grid spacing in x, y, and z directions; min and max refer to minimum and maximum grid spacing within the region of three-dimensional flow.
[b]Δy^+, Δz^+—grid spacing adjacent to flat plate and fin, respectively, in local wall units, i.e., $\Delta y^+ = \Delta y u^*/\nu_w$ where $u^* = (\tau_w/\rho_w)^{1/2}$, τ_w is the local shear stress, ρ_w is the density at the wall, and ν_w is the kinematic molecular viscosity at the wall.

Table 3 Details of conical computations

Case no.	Turbulence model	R/δ_∞[a]	$\Delta\phi_{min}$,[b] $\times 10^3$, deg	$\Delta\phi_{max}$,[b] deg	$\Delta\beta_{min}$[b] $\times 10^3$, deg	$\Delta\beta_{max}$,[b] deg	Δy^+, mean	Δy^+, max	Δz^+, mean	Δz^+, max
3	B-L	29.6	0.77	1.09	1.3	0.96	0.64	1.4	1.6	1.8
4	B-L	38.1	0.60	1.06	1.0	0.98	0.64	1.4	1.6	1.8
5	B-L	38.1	0.60	0.43	1.0	0.44	0.61	1.5	1.7	1.9
6	B-L	38.1	0.60	0.22	1.0	0.20	0.60	1.5	1.7	1.9

[a]R—spherical radius.
[b]$\Delta\beta$, $\Delta\phi$—grid spacing in β and ϕ directions.

Table 4 Details of three-dimensional computation in terms of conical coordinates

Case no.	$\Delta\phi_{min} \times 10^3$, deg	$\Delta\phi_{max}$, deg	$\Delta\beta_{min} \times 10^3$, deg	$\Delta\beta_{max}$, deg
1	0.77	0.89	1.3	1.2
2	0.40	0.80	109.	0.6

$\Delta y^+ \leq 0.8$ for case 2. The number of grid points within the boundary layer on the flat plate was typically 23 for cases 1 and 2, and the number of grid points within the boundary layer on the fin was typically 17 for case 1.

The conical computations (cases 3–6) represent a complete grid-resolution study (Table 3). Cases 4, 5, and 6 incorporate an overall fivefold refinement of the maximum grid spacing $\Delta\beta_{max}$ and $\Delta\phi_{max}$, thereby providing a direct examination of the effects of truncation error. The grid spacing adjacent to the fin and flat plate provided accurate resolution of the viscous sublayers; in particular, $\Delta y^+ \leq 1.5$ and $\Delta z^+ \leq 1.9$. The number of grid points within the boundary layer on the flat plate and fin were typically 22 and 20, respectively. Cases 3 and 4 differ principally in the choice of radius R that provides a check on the conical behavior of the computations. It should be noted that the assumption of conical flow substantially reduces the CPU and computer memory resources required compared with the three-dimensional computations.

The comparable values of grid spacing, expressed in terms of β and ϕ, for cases 1 and 2 at $R = 8.89$ cm measured from the fin leading edge (the location of the experimental measurements of Settles[7]) are given in Table 4. The grid spacing in the conical (β, ϕ) plane is comparable for cases 1, 2, and 3, thereby providing an opportunity for examination of the truncation error of the three-dimensional solution through examination of the conical computations.

Truncation Error Estimates

The grid-resolution study performed for the conical RANS provides an estimate of the truncation error. A grid-independent solution was effectively achieved with case 5. Decreasing the maximum grid spacing by a factor of two from case 5 to 6 resulted in the following maximum changes: 1% in skin friction (except near $\beta = 26$ deg where a small variation in c_f occurs because of an abrupt, unphysical change in the outer turbulence length scale), 2% in surface pressure, and 5% in surface flow direction.[44] Overall, the average changes in c_f, p/p_∞, and Φ from case 5 to 6 were less than 1%. In view of the observed quasiconicality of the three-dimensional computation as discussed below, it is possible to estimate the truncation error of the three-dimensional computations (Baldwin-Lomax) from the measured truncation error of the conical computations. The grid spacing for case 1 was comparable to the coarsest grid employed for the conical computations (cases 3 and 4). The truncation error of the three-dimensional computation is therefore estimated by the maximum difference between cases 4 and 6. These estimates[44] yield a truncation error in the three-dimensional computation of $\pm$ 5% in surface pressure, $\pm$ 10% for Φ, and $\pm$ 15% for c_f.

Results and Discussion

Accuracy of the Theoretical Models

The accuracy of the theoretical models is examined by comparison of the three-dimensional computations with experimental data obtained at a radius of 8.89 cm ($29.6\delta_\infty$) from the fin leading edge. The computed and experimental surface pressures are displayed in Fig. 2. The estimated experimental accuracy is $\pm$ 2.7%. Several experimental flow features (see Fig. 3) are indicated, including the location of the primary separation (β_{ps}) and secondary separation (β_{ss}) based on the surface flow direction, inviscid shock (β_{is}), and primary attachment (β_{pa}). The Baldwin-Lomax model displays closer agreement with experiment in the region 20 deg $< \beta <$ 45 deg, although overestimating the local pressure minimum at $\beta = 32$

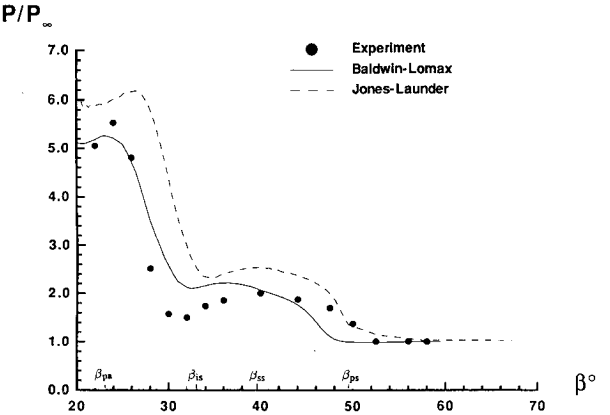

Fig. 2 Computed (three-dimensional) and experimental p/p_∞ at $R = 8.89$ cm from fin leading edge.

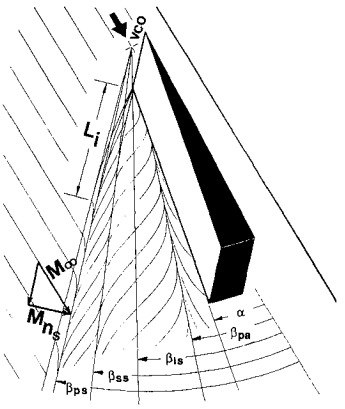

Fig. 3 Definition of surface features for three-dimensional sharp fin.

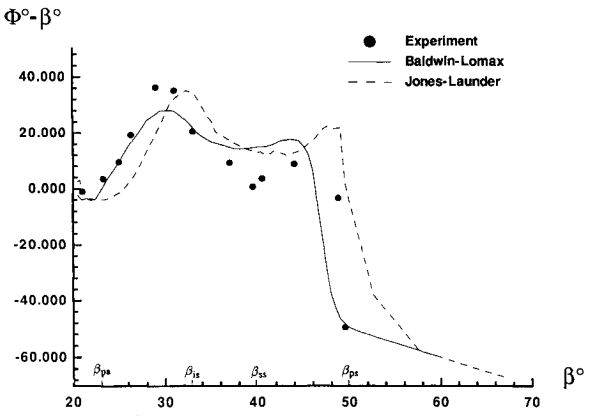

Fig. 4 Computed (three-dimensional) and experimental Φ-β at $R = 8.89$ cm from fin leading edge.

deg by 43%. The Jones-Launder model shows closer agreement with the line of upstream influence, defined as the value of β where the surface pressure begins to rise above the upstream value. Elsewhere, however, the Jones-Launder model shows greater disagreement with the experiment.

The computed and experimental surface flow directions are shown in Fig. 4. The vertical axis Φ-β is the difference between the surface flow direction angle Φ and the angle β relative to the x direction. For conical flows, lines of separation[46] (coalescence) and attachment (divergence) on the flat plate are straight lines through the virtual origin of the conical flow (which is approximately, although not precisely, the fin apex) and therefore can be easily identified as the zeroes of the function Φ-β. The estimated experimental accuracy in Φ is $\pm$ 5%. The Baldwin-Lomax model shows general agreement with experiment; in particular, the angle of the line of separation is predicted within 4%. The predictions using the Jones-Launder model are comparable to the Baldwin-Lomax results. Both theoretical models fail to predict the incipient secondary separation near $\beta = 40$ deg.

Quasiconical Behavior of Three-Dimensional Computation

Because of the similarity of the computations using the Baldwin-Lomax and Jones-Launder models, the conical behavior of the computed flowfield is examined using results obtained with the Baldwin-Lomax model only. Examination of the quasiconical behavior of the flowfield requires the determination of the VCO of the experiment and computation. Conceptually, any function of v, p, and/or T may be used. The experimental data exhibit a VCO located at the intersection of 1) a surface feature (e.g., the line of separation or surface isobars), and 2) the extension of the inviscid shock. According to this method, which recognizes the role of the inviscid shock in defining the general location of the interaction, the experimental VCO was located at 2.1 cm $\pm$ 0.3 cm forward of the fin leading edge along an extension of the inviscid shock.

The computed VCO was determined by the intersection of 1) a surface feature (as earlier), and 2) the extension of the fin surface. This method recognizes the requirement that the fin surface lie on a conical ray of the conical computations. Although this method differs from the technique used for the experimental data, the conclusions reached herein would not change significantly were the experimental method employed.[45] The computed flowfield displays a range of locations for the VCO. The intersection of surface isobars, selected from the vicinity of the inviscid shock, with a line parallel to the fin surface, yields a VCO at $(x, y, z) = (0, 0, 0)$ denoted as VCO_0. The interaction of surface isobars, selected from the vicinity of the line of upstream influence, with a line parallel to the fin, yields a VCO at $(x, y, z) = (x_\Delta, 0, z_\Delta)$, denoted as VCO_Δ, at distance $\Delta = 2.5$ cm $(8.5\delta_\infty)$ from the fin leading edge, which is within 0.7 cm of the experimental VCO. Notwithstanding the variation in the VCO, the linearity of the surface isobars outside of an initial inception zone near the fin leading edge indicates conical symmetry of the surface pressure.[45]

The computed surface pressure p/p_∞ at three radii are displayed in Fig. 5 together with the experimental data. The transverse angle $\tilde{\beta} = \tan^{-1}[(z-z_\Delta)/(x-x_\Delta)]$. The computed surface pressure displays conical behavior, i.e., the p/p_∞ becomes independent of R at increasing values of R. The computed surface flow direction is displayed in Fig. 6 at three radii. The computed Φ-β displays conical behavior, i.e., the

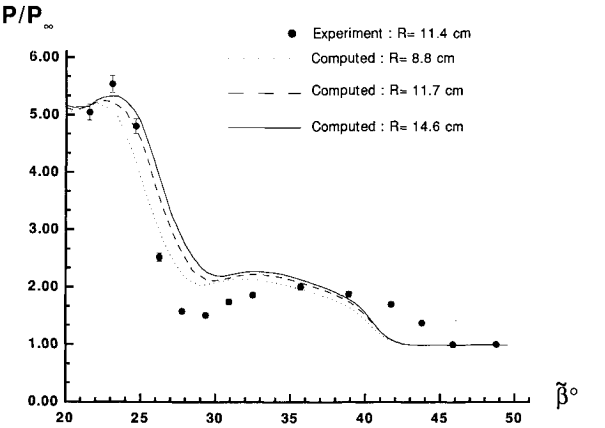

Fig. 5 Computed (three-dimensional) and experimental p/p_∞ using VCO_Δ.

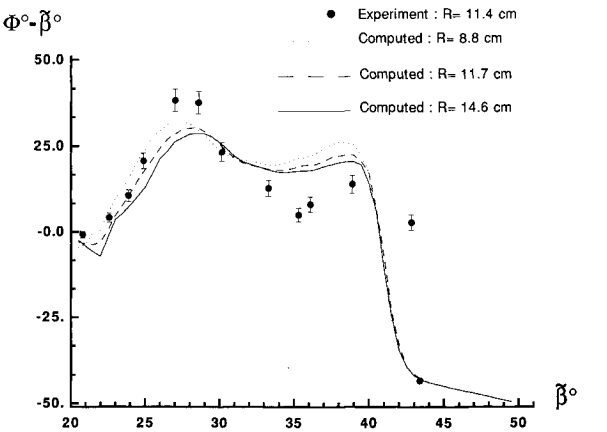

Fig. 6 Computed (three-dimensional) and experimental Φ-β using VCO_Δ.

Φ-β profile becomes independent of R at increasing values of R. The computed values of $c_f R/\delta_\infty$ are presented in Fig. 7 at three radii, together with the experimental data for one radius. The computed skin friction does not exhibit conical behavior, i.e., $c_f R/\delta_\infty$ is not independent of R. Indeed, the computed c_f asymptotes to a constant value for increasing R.

The computed "conical" streamlines at $R = 29.2\delta_\infty$ and $48.5\delta_\infty$, obtained using VCO_Δ, are shown in Figs. 8a and 8b. (The conical streamlines were also examined using VCO_0, and similar results were obtained as described later.[45]) The conical streamlines are determined by the velocity components $u_{\tilde{\beta}}$ and u_ϕ that are obtained from the full three-dimensional Cartesian velocity $v = (u, v, w)$ according to $u_\phi = -u \sin\phi \cos\tilde{\beta} + v \cos\phi - w \sin\phi \sin\tilde{\beta}$ and $u_{\tilde{\beta}} = -u \sin\tilde{\beta} + w \cos\tilde{\beta}$. If the three-dimensional velocity field is conical, these conical streamlines will appear identical at all R. Qualitatively, the streamlines are very similar. The primary vortex (including separation and attachment line) and secondary corner vortex (including separation line) are similar. The primary attachment line occurs at approximately the same $\tilde{\beta}$ location, i.e., $\tilde{\beta}_{pa} = 21.5$ deg at $R = 29.2\delta_\infty$ (Fig. 8a) and $\tilde{\beta}_{pa} = 23.3$ deg at $R = 48.5\delta_\infty$ (Fig. 8b). However, the path of the attachment streamline (indicated by an arrow) varies significantly for the two values of R, indicating its sensitivity to small deviations from conicity in the vicinity of the line of attachment. The attachment streamline appears to approach the shape obtained from the conical calculation (Fig. 9) with increasing R. However, a definitive statement is not possible because of the limited size of the three-dimensional computational domain. (The largest radius, $R = 48.5\delta_\infty$, represents the limit of the three-dimensional computational domain.) Density, Mach number, and static and total pressure have also been examined[45] at several radii using contour plots and were found to display conical behavior.

In summary, the computed three-dimensional flowfield is quasiconical. Several surface variables (e.g., surface pressure and surface flow direction) and flowfield variables (including density, Mach number, and static and total pressure) exhibit conical behavior. The computed surface skin friction, however, does not display conical behavior. Also, although the computed streamlines are qualitatively similar at different radii, the attachment streamline does not exhibit conical behavior within the region examined. Notwithstanding the described departures from exact conicity, the examination of the computed and experimental flowfields in the conical framework provides substantial insight to the flowfield structure as described later.

Since the computed three-dimensional flowfield shows quasiconical behavior, it is expected that the three-dimensional and conical computations would yield similar results. This has been confirmed[45] through detailed comparison of surface pressure, flow direction, and skin friction for the three-dimensional and conical computations.

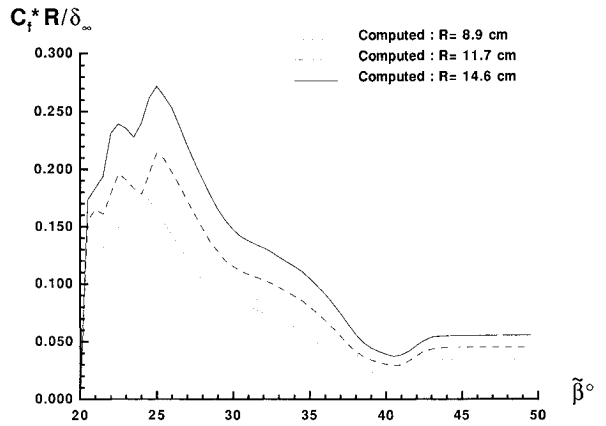

Fig. 7 Computed (three-dimensional) and experimental c_f using VCO_Δ.

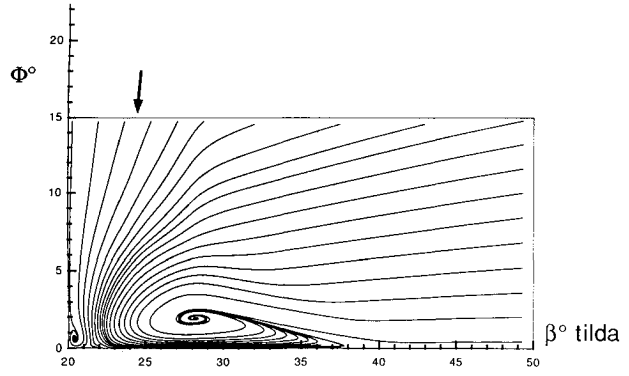

Fig. 8a Conical streamlines at $R = 29.2\delta_\infty$ from (three-dimensional) computation using VCO_Δ.

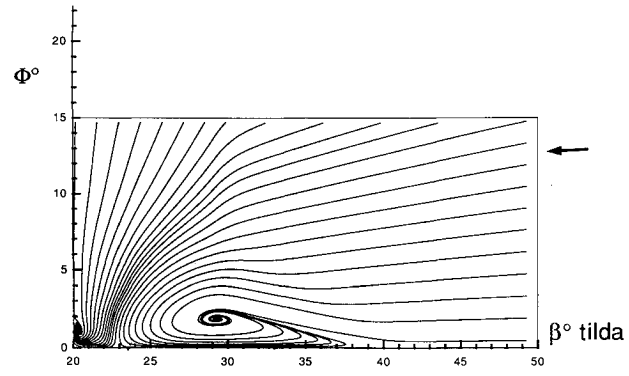

Fig. 8b. Conical streamlines at $R = 48.5\delta_\infty$ from (three-dimensional) computation using VCO_Δ.

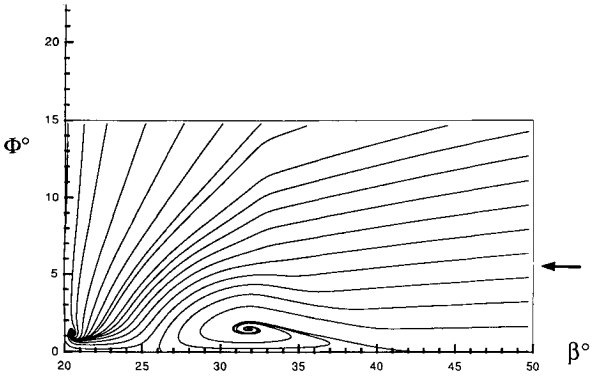

Fig. 9 Conical streamlines from conical calculation.

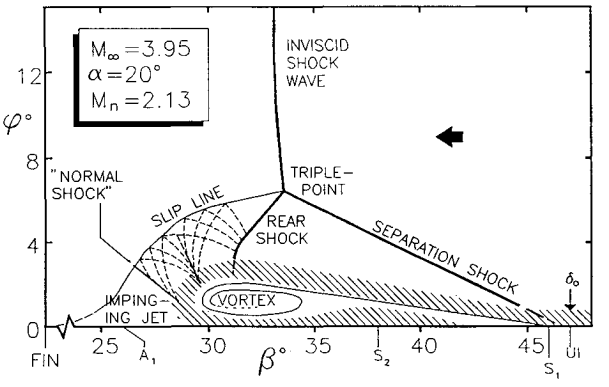

Fig. 10 Flowfield model of Alvi and Settles.[35,36]

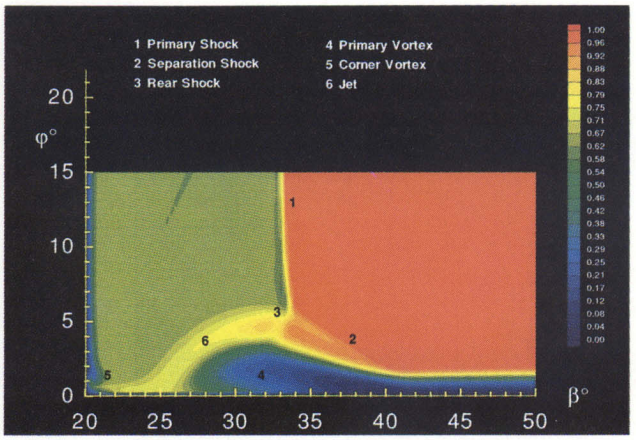

Fig. 11 Computed (conical) total pressure $p_t/p_{t\infty}$.

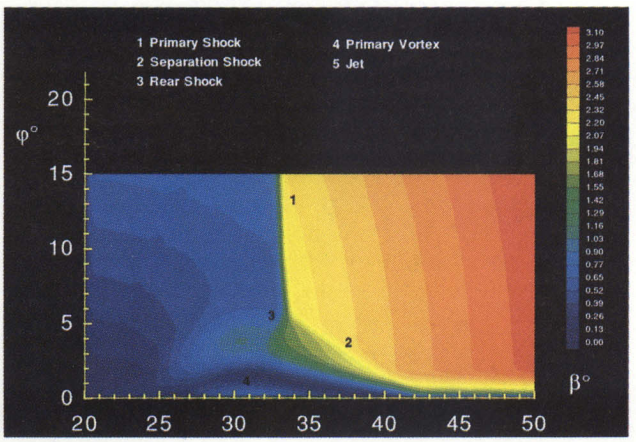

Fig. 12 Computed (conical) normal Mach number M_n.

Flowfield Structure

Alvi and Settles[35,36] have developed a detailed flowfield model for the three-dimensional single fin interaction (Fig. 10) based on the quasiconical behavior that has been observed both experimentally and computationally. A qualitative model was developed earlier by Zheltovodov and Shilein,[4] and detailed comparison of these models was performed by Hsu and Settles.[25]

The increased grid resolution achieved in the conical computations permits a detailed comparison with the flowfield model of Settles et al. The flowfield structure is observed in the computed contour plots for total pressure $p_t/p_{t\infty}$ (Fig. 11), normal Mach number M_n (Fig. 12), defined by $M_n = [(u_\beta^2 + u_\phi^2)/\gamma RT]^{1/2}$, static pressure p/p_∞ (Fig. 13), and density ρ/ρ_∞ (Fig. 14). Each of these contour plots highlights specific flowfield features. Experimental[26] results for density ρ/ρ_∞ (Fig. 15) are also shown.

The conical computed flowfield displays general agreement with the model of Alvi and Settles[35,36] and is similar to the three-dimensional computed flowfield.[44] The λ shock (formed by the main, separation, and rear shocks) is evident in all contour plots, particularly the density plots. The computed ϕ location of the triple point $\phi_{TP} = 5.8$ deg is in good agreement with the experimental[36] value $\phi_{TP} = 6.5$ deg. A slip line, emanating from the triple point, is visible in the total pressure contours. The slip line approaches the flat plate at a location between the line of attachment and the corner. The large primary vortex is a dominant feature of the flowfield. The vortex is defined by the separation and attachment streamlines. The computed conical attachment streamline (Fig. 9) is located at $\phi_{AS} = 4.6$ deg at the computed separation line ($\beta_{ps} = 42$ deg) and is above the boundary layer δ_∞ located at $\phi = 2$ deg. This is qualitatively consistent with the experimental observation that the attachment streamline originates outside the edge of the incoming boundary layer.[36] This observation has important implications for high-speed inlet design since in this case the entire incoming turbulent boundary layer is entrained into the primary vortex that is oriented approximately along the inviscid shock line.

The density contours (Figs. 14 and 15) indicate that the computed primary vortex is smaller than the experiment. This observation explains the underestimate in the upstream influence line (Fig. 3). This discrepancy is attributable to the turbulence model. A similar underestimate of the vortex size is observed for the Jones-Launder model. The computed static pressure contours display an expansion region associated with the turning of the flow over the primary vortex. A portion of the expansion is conically supersonic with normal Mach number M_n slightly larger than one. A high total pressure "jet" emanates from the flow processed through the λ shock structure and impinges on the flat plate between the fin and line of attachment. This jet is an essential element in the production of high skin friction in the vicinity of the line of attachment.

There are several differences between the conical computations at Mach 4 and $\alpha = 20$ deg and the flowfield model of Settles et al. The computations do not exhibit a "normal" shock in the vicinity of the flat plate nor the transonic "shocklets" in the expansion region. This discrepancy may be attributable to differences between the size and shape of computed and experimental primary vortex, A larger primary vortex may result in an increased curvature of the computed attachment streamline in the region between the line of attachment and inviscid shock. The increased curvature would imply a greater expansion of the flow around the vortex, resulting in higher Mach numbers and possibly a normal shock. The dis-

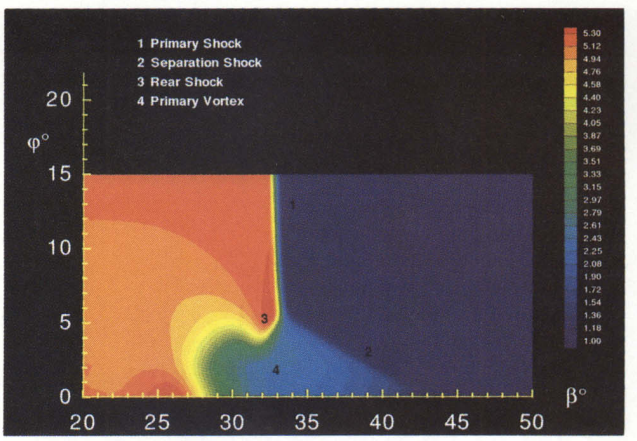

Fig. 13 Computed (conical) static pressure p/p_∞.

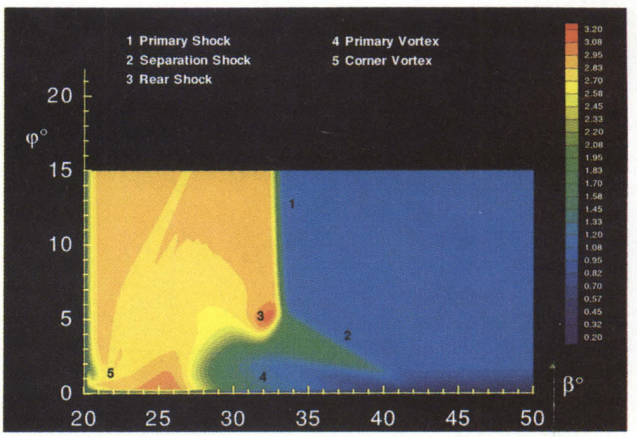

Fig. 14 Computed (conical) density ρ/ρ_∞.

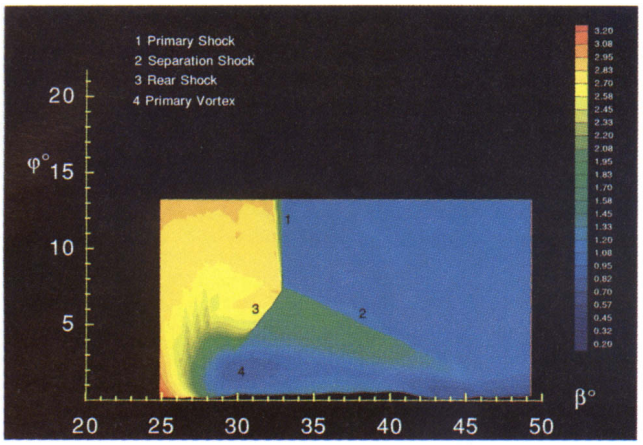

Fig. 15 Experimental density ρ/ρ_∞.

crepancies in the size and shape of the computed and experimental vortex are attributable to the limitations of the turbulence model. The computations do not exhibit an incipient secondary separation that is observed in the experiment (Fig. 4). The absence of this feature is probably due to the absence of an adverse ($\partial p/\partial\beta > 0$) pressure gradient in the computation for 30 deg $< \beta <$ 35 deg (Fig. 3), which is again attributable to the limitations of the turbulence model. A small secondary corner vortex is evident in the computations, although its quantitative accuracy is suspect because of the limitations of the turbulence model in the corner region. A secondary corner vortex has been observed by several investigators.[5,47]

Overall, the computed flowfield shows strong agreement with the model of Alvi and Settles.[35,36] Although the observed quasiconicity precludes an exact conical treatment of the flowfield, the conical model is a powerful tool for understanding the fluid physics of this interaction and its relevance is confirmed by both experiment and theory.

Conclusions

A series of computations have been performed for the three-dimensional single fin interaction at Mach 4, $\alpha = 20$ deg, and $Re_{\delta\infty} = 2.18 \times 10^5$ using the three-dimensional and conical Reynolds-averaged Navier-Stokes equations with turbulence incorporated using the Baldwin-Lomax and Jones-Launder models. The computed flowfields obtained from the Baldwin-Lomax and Jones-Launder models are similar. The computed surface pressure and surface flow angle are in general agreement with the experimental data of Kim et al.[7] The computed density contours underestimate the size of the primary vortex. The underestimate is believed because of the turbulence model.

The computed three-dimensional flowfield is quasiconical. The surface pressure, surface flow direction, and flowfield contours of static pressure, density, and Mach number are approximately conical over the extent of the computational domain, except for an inception region near the fin leading edge. The surface skin friction does not exhibit conical behavior in this range. The conical streamlines are qualitatively similar at different radii R; however, certain features (e.g., the path of the attachment streamline) are not conical because of sensitivity to small deviations of the three-dimensional velocity field from conicity.

The computed flowfield exhibits most of the features of the model of Alvi and Settles, including the λ shock, slip line, primary vortex, expansion, and high-speed jet. Several flowfield parameters showed good quantitative agreement with experiment. The computations do not exhibit the normal shock, transonic shocklets, and secondary separation observed in the experiment. This discrepancy may be attributable to the underestimate of the size of the primary vortex because of limitations of the turbulence model.

Acknowledgments

This research was sponsored by the Air Force Office of Scientific Research under Grants 86-0266 and 89-0315, monitored by Len Sakell, and by the NASA Ames Research Center. Computations were performed at the John von Neumann National Supercomputer Center and the NASA Ames Research Center. Analysis of the flowfields was performed at the Rutgers University, College of Engineering Supercomputer Remote Access Center, sponsored by Rutgers University.

References

[1]Settles, G. S., and Dolling, D. S., "Swept Shock Wave Boundary Layer Interactions," *Tactical Missile Aerodynamics*, edited by M. J. Hemsch and J. N. Nielsen, Vol. 104, Progress in Astronautics and Aeronautics, AIAA, New York, 1986, pp. 297–379.

[2]Settles, G. S., and Dolling, D. S., "Swept Shock/Boundary-Layer Interactions—Tutorial and Update," AIAA Paper 90-0375, AIAA 28th Aerospace Sciences Meeting, Jan. 1990.

[3]Zheltovodov, A., Maksimov, A., and Shilein, E., "Development of Turbulent Separated Flows in the Vicinity of Swept Shock Waves," *The Interactions of Complex 3-D Flows*, Inst. of Theoretical and Applied Mechanics, USSR Academy of Sciences, Novosibirsk, Russia, 1987, pp. 67–91.

[4]Zheltovodov, A., and Shilein, E., "Three Dimensional Interaction of Swept Shock Waves with Turbulent Boundary Layer in Corner Configurations," Inst. of Theoretical and Applied Mechanics, Preprint 34-86, USSR Academy of Sciences, Novosibirsk, Russia, 1986 (in Russian).

[5]Zheltovodov, A. A., Dvorak, R., and Safarik, P., "The Features of Shock Wave-Turbulent Boundary Layer Interactions at Transonic and Supersonic Conditions," *Proceedings of the Siberian Board of the USSR Academy of Sciences*, Vol. 6, 1990 (in Russian).

[6]Kim, K.-S., and Settles, G. S., "Skin Friction Measurements by Laser Interferometry in Swept Shock Wave/Turbulent Boundary Layer Interactions," AIAA Paper 88-0497, Jan. 1988; also *AIAA Journal*, Vol. 28, No. 1, 1990, pp. 133–139.

[7]Kim, K.-S., Lee, Y., Alvi, F., Settles, G. S., and Horstman, C. C., "Skin Friction Measurements and Computational Comparison of Swept Shock/Boundary-Layer Interactions," *AIAA Journal*, Vol. 29, No. 10, 1991, pp. 1643–1650.

[8]Kubota, H., and Stollery, J. L., "An Experimental Study of the Interaction Between a Glancing Shock Wave and a Turbulent Boundary Layer," *Journal of Fluid Mechanics*, Vol. 116, March 1982, pp. 431–458.

[9]Law, C. H., "Three-Dimensional Shock Wave-Turbulent Boundary Layer Interactions at Mach 6," Aerospace Research Lab., ARL-TR-75-0191, Wright-Patterson AFB, OH, June 1975.

[10]McClure, D., and Dolling, D. S., "Flowfield Scaling in Sharp-Fin Induced Shock Wave Turbulent Boundary Layer Interaction," AIAA Paper 83-1754, July 1983.

[11]Oskam, B., Vas, I., and Bogdonoff, S. M., "Mach 3 Oblique Shock Wave/Turbulent Boundary Layer Interactions in Three Dimensions," AIAA Paper 76-336, July 1976.

[12]Oskam, B., Vas, I., and Bogdonoff, S. M., "An Experimental Study of Three-Dimensional Flow Fields in an Axial Corner at Mach 3," AIAA Paper 77-689, June 1977.

[13]Shapey, B., and Bogdonoff, S. M., "Three-Dimensional Shock Wave-Turbulent Boundary Layer Interaction for a 20 Deg Sharp Fin at Mach 3," AIAA Paper 87-0554, Jan. 1987.

[14]Horstman, C. C., and Hung, C. M., "Computation of Three-Dimensional Separated Flows at Supersonic Speeds," AIAA Paper 79-0002, Jan. 1979.

[15]Knight, D., "A Hybrid Explicit-Implicit Numerical Algorithm for the Three-Dimensional Compressible Navier-Stokes Equations," *AIAA Journal*, Vol. 22, No. 8, 1984, pp. 1056–1061.

[16]Knight, D., "Modelling of Three-Dimensional Shock Wave Turbulent Boundary Layer Interactions," Workshop on Macroscopic Modelling of Turbulent Flows and Fluid Mixtures, INRIA, Nice, France, Dec. 1984; see also *Lecture Notes in Physics,* Vol. 230, Springer-Verlag, New York, 1985, pp. 177–201.

[17]Knight, D., "Calculation of Three-Dimensional Shock/Turbulent Boundary Layer Interaction Generated by a Sharp Fin," *AIAA Journal*, Vol. 23, No. 12, 1985, pp. 1885–1891.

[18]Knight, D., "Numerical Simulation of a Three-Dimensional Shock Wave-Turbulent Boundary Layer Interaction Generated by a Sharp Fin at Mach 4," *Computer Systems in Engineering*, Vol. 1, Nos. 2–4, 1990, pp. 391–399.

[19]Knight, D., Horstman, C. C., Shapey, B., and Bogdonoff, S. M., "Structure of Supersonic Flow Past a Sharp Fin," *AIAA Journal*, Vol. 25, No. 10, 1987, pp. 1331–1337.

[20]Gaitonde, D., and Knight, D., "Numerical Experiments on the 3-D Shock Wave-Boundary Layer Interaction Generated by a Sharp Fin," AIAA Paper 88-0309, Jan. 1988.

[21]Gaitonde, D., and Knight, D., "Numerical Investigation of Bleed on Three-Dimensional Turbulent Interactions Due to Sharp Fins," *AIAA Journal*, Vol. 29, No. 11, 1991, pp. 1878–1885.

[22]Baldwin, B., and Lomax, H., "Thin Layer Approximation and Algebraic Model for Separated Turbulent Flows," AIAA Paper 78-257, Jan. 1978.

[23]Cebeci, T., and Smith, A., *Analysis of Turbulent Boundary Layers*, Academic Press, New York, 1974.

[24]Jones, W., and Launder, B., "The Prediction of Laminarization with a Two-Equation Model of Turbulence," *International Journal of Heat and Mass Transfer*, Vol. 15, 1972, pp. 301–304.

[25]Hsu, J. C., and Settles, G. S., "Measurements of Swept Shock Wave-Turbulent Boundary Layer Interactions by Holographic Interferometry," AIAA Paper 89-1849, June 1989.

[26]Hsu, J. C., and Settles, G. S., "Holographic Flowfield Density Measurements in Swept Shock Wave/Boundary Layer Interactions," AIAA Paper 92-0746, Jan. 1992.

[27]Stanbrook, A., "An Experimental Study of the Glancing Interaction Between a Shock Wave and a Boundary Layer" British Aeronautical Research Council, ACR CP-555, July 1960.

[28]Lowrie, B., "Cross-Flows Produced by the Interaction of a Swept Shock Wave with a Turbulent Boundary Layer," Ph.D. Thesis, Cambridge Univ., Cambridge, England, UK, Dec. 1965.

[29]McCabe, A., "The Three-Dimensional Interaction of a Shock Wave with a Turbulent Boundary Layer," *Aeronautical Quarterly*, Vol. 17, Aug. 1966, pp. 231–252.

[30]Token, K., "Heat Transfer Due to Shock Wave/Turbulent Boundary Layer Interactions on High Speed Weapons Systems," Air Force Flight Dynamics Lab., AFFDL-TR-74-77, Wright-Patterson AFB, OH, 1974.

[31]Zheltovodov, A. A., "Properties of Two- and Three-Dimensional Separation Flows at Supersonic Velocities," *Proceedings of the USSR Academy of Sciences, Mechanics of Liquids and Gasses*, Vol. 14, May–June 1979, pp. 42–50.

[32]Knight, D., Horstman, C. C., Ruderich, R., Mao, M.-F., and Bogdonoff, S. M., "Supersonic Turbulent Flow Past a 3-D Swept Compression Corner at Mach 3," AIAA Paper 87-0551, Jan. 1987.

[33]Knight, D., Raufer, D., Horstman, C. C., Ketchum, A., and Bogdonoff, S. M., "Supersonic Turbulent Flow Past a 3-D Swept Compression Corner at Mach 3: Part II," AIAA Paper 88-0310, Jan. 1988.

[34]Lu, F., and Settles, G. S., "Structure of Fin-Shock/Boundary Layer Interactions by Laser Light-Screen Visualization," AIAA Paper 88-3801, July 1988.

[35]Alvi, F., and Settles, G. S., "Structure of Swept Shock Wave/Boundary Layer Interactions Using Conical Shadowgraphy," AIAA Paper 90-1644, June 1990; *AIAA Journal* (submitted for publication).

[36] Alvi, F., and Settles, G. S., "A Physical Model of the Swept Shock/Boundary Layer Interaction Flowfield," AIAA Paper 91-1768, June 1991.

[37]Rubesin, M., and Rose, W., "The Turbulent Mean-Flow, Reynolds-Stress and Heat-Flux Equations in Mass Averaged Dependent Variables," NASA TMX-62248, March 1973.

[38]Pulliam, T., and Steger, J., "Implicit Finite-Difference Simulations of Three-Dimensional Compressible Flow," *AIAA Journal*, Vol. 18, No. 2, 1980, pp. 159–167.

[39]Hung, C. M., and MacCormack, R. W., "Numerical Solution of Three-Dimensional Shock Wave and Turbulent Boundary Layer Interaction,"*AIAA Journal*, Vol. 16, No. 10, 1978, pp. 1090–1096.

[40]Ames Research Staff, *Equations, Tables and Charts for Compressible Flow*, Rept. 1135, National Advisory Committee for Aeronautics, Moffett Field, CA, 1953, Eq. (A3), p. 19.

[41]MacCormack, R. W., "Numerical Solution of the Interaction of a Shock Wave with a Laminar Boundary Layer," *Lecture Notes in Physics*, Vol. 8, Springer-Verlag, New York, 1971, pp. 151–163.

[42]Keller, H. B., "Accurate Difference Methods for Nonlinear Two-Point Boundary Value Problems," *SIAM Journal of Numerical Analysis*, Vol. 11, No. 2, 1974, pp. 305–320.

[43]MacCormack, R. W., "A Numerical Method for Solving the Equations of Compressible Viscous Flow," *AIAA Journal*, Vol. 20, No. 9, 1982, pp. 1275–1281.

[44]Knight, D., Settles, G. S., and Horstman, C. C., "Three Dimensional Shock Wave Turbulent Boundary Layer Interactions Generated by a Sharp Fin at Mach 4," AIAA Paper 91-0648, Jan. 1991.

[45]Knight, D., and Badekas, D., "On the Quasi-Conical Flowfield Structure of the Swept Shock Wave-Turbulent Boundary Layer Interaction," AIAA Paper 91-1759, June 1991.

[46]Lighthill, M., *Laminar Boundary Layers*, edited by L. Rosenhead, Oxford Univ. Press, Oxford, England, UK, 1963, pp. 72–82.

[47]Zheltovodov, A. A., private communication, July 1990.